Hindawi
Advances in Civil Engineering
Volume 2019, Article ID 1413568, 14 pages
https://doi.org/10.1155/2019/1413568

Research Article

Research on the Deformation Characteristics and Support Technology of a Bottom Gas Extraction Roadway under Repeated Interference

Rongkun Pan,[1] Zhihui Ma,[1,2] Minggao Yu,[1] and Shuaidong Wu[2]

[1]*College of Safety Science and Engineering, Henan Polytechnic University, Jiaozuo 454000, China*
[2]*Production Technology Department, Yima Coal Industry Group Co., Ltd, Sanmenxia 472300, China*

Correspondence should be addressed to Zhihui Ma; huaer702@163.com

Received 16 April 2019; Revised 7 June 2019; Accepted 29 June 2019; Published 29 August 2019

Academic Editor: Alessandro Palmeri

Taking Pingbao Coal Mine as the engineering background, the stress distribution, surrounding rock displacement, and plastic zone distribution characteristics of a bottom gas extraction roadway are simulated by FLAC3D under multiple disturbances. The mining disturbance due to the overlying coal seam is obtained: the deformation of the roof subsidence and lower rib closure of the bottom gas extraction roadway are larger than the floor heave and upper rib closure, respectively. According to the mechanical analysis of the bottom gas extraction roadway, the equations for calculating the displacement at each point on the surface of the bottom gas extraction roadway and the methods for calculating the maximum displacement, the maximum normal stress, and the maximum shear stress are obtained to reasonably explain the deformation of the bottom gas extraction roadway under multiple disturbances. Then, the bolt-mesh-anchor and ladder beam support mode are designed. After onsite observation of the bottom gas extraction roadway of the 12030 coal mining face of the Pingbao Coal Mine, it is concluded that the deformation characteristics of the bottom gas extraction roadway basically conform to the abovementioned equations and that the support is effective. This paper can provide a reference for the optimization of bottom gas extraction roadway positioning, the determination of support parameters, and the deformation prediction around a bottom gas extraction roadway under similar conditions.

1. Introduction

At present, there are two main measures to prevent outburst at coal mining faces: one is to exploit protective seams and the other is to predrain coal seam gas [1]. For mines without protective seams to mine, the predraining coal seam gas is generally used as the main means of regional outburst prevention. The main principle of this method is that after the completion of the construction of the bottom gas extraction roadway, a certain number of extraction holes are drilled from the roof of the bottom gas extraction roadway to predrain gas from the overlying coal seam [2, 3]. When the coal seam is no longer at risk of outburst, a gas control measure of the coal extraction roadway is implemented, so the bottom gas extraction roadway provides protection during coal roadway excavation. However, in the process of coal roadway excavation and working face mining, the bottom gas extraction roadway is disturbed repeatedly, which destroys the structure and stability of the roadway surrounding rock and causes the bolts and anchor cables to undergo changes in their stress state or even fail; these effects are manifested as deformation, subsidence, and destruction of the bottom gas extraction roadway [4]. The deformation of the bottom gas extraction roadway is mainly related to the transfer of abutment pressure in the floor caused by coal seam disturbance. The deformation characteristics of bottom gas extraction roadways vary with the location of the roadway. To reasonably select the control mode of the surrounding rock of the bottom roadway, it is necessary to understand the deformation characteristics of the bottom roadway during different disturbance periods [5].

At present, mining scholars have carried out pioneering research on stress transfer in floors, surrounding rock deformation, and floor extraction roadway failure mechanisms

and have made some progress. On the basis of mine pressure, Zhu et al. [6] concluded that with the advancing of the working face, the range of the change in floor stress at a fixed position decreases with depth, and the direction of maximum principal stress changes from vertical to horizontal. Santos and Bieniawski [7] and Afrouz et al. [8] discussed the stress state at a certain point in the floor during coal seam mining. Gong et al. [9] simulated the mining process of the working face by using a three-dimensional simulation test bench. It was concluded that the displacement and stress changed most dramatically 10–15 m from the coal floor. Guan et al. [10] simulated the stress distribution and failure state of floors in multiseam mining. Xie et al. [11, 12] believe that after mining in an upper coal seam, the floor stress will redistribute, and the newly formed stress concentration will transfer to the deep floor, resulting in a sharp increase in floor roadway deformation. Zhang et al. [13] combined Coulomb–Mohr strength theory and Griffith strength theory to obtain the maximum floor failure depth under mining influence. Sun [14] numerically simulated the influence of coal seam dip on floor failure depth, failure form, and maximum failure depth. Zhou et al. [15] discussed the influence law of floor mining on the mining face and obtained an equation for calculating the maximum depth of the floor mining fracture zone. Zhang et al. [16] established an elastic-plastic mechanical model of a cross-mining pressure roadway and analysed the stress distribution law of the roadway and the deformation characteristics of the surrounding rock for mining in different overlying coal seams. Zhang et al. [17] used the nonlinear finite element method to analyse the stress distribution law of different pillar widths in the floor rock and then obtained a method to determine a reasonable position of the lower coal seam mining roadway. According to a similar material simulation experiment, reasonable layout parameters of a floor roadway were obtained by Zhang et al. [18].

However, these research results mainly focus on the stress transmission under the floor and the destruction of the floor roadway under the influence of static pressure, while few studies have been conducted on the deformation characteristics of the floor roadway under the influence of multiple disturbances. A bottom gas extraction roadway is affected by not only the disturbance of its own excavation but also the disturbance of overlying coal seam mining. The deformation characteristics of a roadway are complex [19]. Therefore, it is not feasible to explain these phenomena with traditional theoretical approaches under the influence of static pressure. Carrying out research on the deformation characteristics of bottom gas extraction roadways under multiple disturbances has a certain theoretical significance and practical value.

In this paper, the factors and evolution of the deformation and instability of a bottom gas extraction roadway are briefly described. The deformation law of a bottom gas extraction roadway under multiple disturbances is summarized through stress analysis and numerical simulation analysis of a bottom gas extraction roadway. Field observations were collected from the Pingbao Coal Mine, and support technology was then applied in this coal mine.

2. Numerical Simulation and Analysis of the Surrounding Rock Deformation during Bottom Roadway Excavation

2.1. Factors and Evolution of the Deformation and Instability of a Bottom Gas Extraction Roadway. The deformation and instability of a bottom gas extraction roadway are mainly related to the physical and mechanical properties and geological conditions of the surrounding rock, the supporting form of the roadway, and the timing of the disturbances to the bottom gas extraction roadway.

According to the structural change and stress distribution in the surrounding rock, the process of structural instability of the surrounding rock under the influence of mining can be simply divided into the following two stages (Figure 1):

(1) Excavation disturbance stage of bottom gas extraction roadway: after excavation of the bottom gas extraction roadway, stress concentration will occur in some parts of the roadway surrounding rock. When the stress in the surrounding rock is less than the value of concentrated stress, the rock will be destroyed and the stress will transfer to the deeper rock. The concentrated stress will reach equilibrium at a certain location, and the roadway will tend to stabilize [19].

(2) Disturbance stage of coal seam mining: during upper coal seam mining, the bottom gas extraction roadway is disturbed again, mainly due to three disturbances, namely, excavation on the coal roadway, mining of the upper coal face, and mining of the lower coal face. Under these additional stress disturbances, cracks are induced in the surrounding rock of the roadway. These structural cracks further promote energy release and activate other cracks. The stress then redistributes. With time, as the disturbance weakens, the stress shifts to deeper surrounding rock and reaches equilibrium again. Because the bottom gas extraction roadway will no longer be used after the mining of the lower section of the coal face, the disturbance of the bottom gas extraction roadway caused by the mining of the lower section of the coal face will not be considered in the following analysis. Therefore, the bottom gas extraction roadway studied in this paper is disturbed by three times, that is, the first disturbance after the bottom gas extraction roadway is excavated, the second disturbance after the coal roadway is excavated, and the third disturbance after the upper coal face is excavated.

2.2. Numerical Simulation and Analysis. Pingbao Coal Mine is a gas outburst mine. Considering the geological conditions, gas extraction, borehole engineering quantity, and engineering analogy, the following layout forms are adopted in Pingbao Coal Mine. The vertical distance between bottom gas extraction roadway and coal seam is 10 m, the horizontal distance between bottom gas extraction roadway and coal

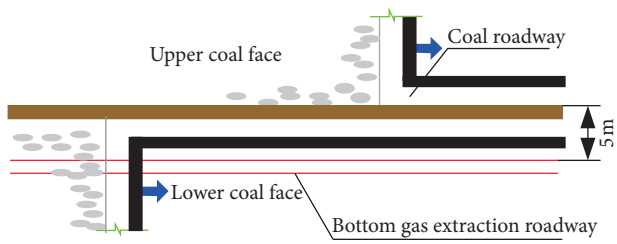

Figure 1: Diagram of disturbance in bottom gas extraction roadway. The figure is a top view, and the bottom gas extraction roadway is located in the floor. The order of disturbance is bottom gas extraction roadway excavation, coal roadway excavation, and upper coal face excavation.

roadway is 5 m, and the bottom gas extraction roadway has an outward staggered arrangement. The layout form has been proved to be the optimal layout of the bottom gas extraction roadway in this mine.

FLAC3D numerical simulation software is used to simulate the stress distribution and deformation characteristics of the bottom gas extraction roadway under various disturbances in Pingbao Coal Mine [20]. The rock mechanics parameters are shown in Table 1.

In the Cartesian coordinate system, the calculation model is set as follows: the horizontal direction perpendicular to the roadway is x axis, parallel to the roadway direction is y-axis, and the vertical direction in the roadway is z-axis. According to the coordinate system, the calculation model range is 200 m × 100 m × 55 m. In order to simplify the model and make the calculation faster, the grid of X is encrypted in the range of 76 m to 134 m. The schematic diagram of the calculation model is shown in Figure 2.

2.2.1. Stress and Deformation Law of the Surrounding Rock after Excavation of a Bottom Gas Extraction Roadway. The stress distribution, displacement field, and plastic zone of the surrounding rock after the excavation of the bottom gas extraction roadway are shown in Figure 3.

Figure 3(a) shows that due to the vertical stress, a stress concentration area is formed in either rib of the roadway after excavation. The stress concentration coefficient is 1.55. The surrounding rock within a certain range from the roadway surface is broken, and a stress reduction area is formed. After the roadway stabilizes, the stress reduction area located in the roof and floor of the roadway presents a spherical shape, encompassing a larger range. Figure 3(b) shows that due to the horizontal stress, a large stress reduction zone appears in either rib of the roadway after the excavation of the bottom gas extraction roadway, and stress concentration zones also appear on the roof and floor of the roadway. During the process of roadway stability, the stress concentration zones of the roof and floor continue to expand, and the stress distributions at the two ribs remain basically unchanged. Figure 3(c) shows that with the increase in shear force after the excavation of the bottom gas extraction roadway, a shear stress concentration area is formed at each of the four corners of the roadway. According to the principle of shear stress equilibrium, distributions of shear stress form pairs, creating a butterfly-like shape at the four corners of the roadway, while the direction of the shear stress in the adjacent two ribs is opposite. After the roadway is stable, the roof upper corner and the floor lower corner of the roadway are affected by the shear stress. The maximum shear stress is 8 MPa, and the stress concentration occurs at a depth of 1 m from the surrounding rock. Figure 3(d) shows that the surrounding rock moves towards the goaf direction and that the roof subsides considerably after the bottom gas extraction roadway is excavated. Figure 3(e) shows that there is a plastic zone extending approximately 1-2 m into the surrounding rock of two ribs of the roadway, and the plastic zone of the roof and floor extends 1.5–2.5 m into the surrounding rock.

2.2.2. Stress and Deformation Law of the Surrounding Rock of a Bottom Gas Extraction Roadway after Coal Roadway Excavation. After coal roadway excavation, secondary disturbance of the bottom gas extraction roadway occurs. The stress field, plastic zone extent, and displacement field of the surrounding rock of the bottom gas extraction roadway are redistributed, as shown in Figure 4.

Figure 4(a) shows that the vertical stress redistribution at the bottom gas extraction roadway is affected by the excavation of the coal roadway. Excavation of the coal roadway unloads the roof and lower rib of the bottom gas extraction roadway, and the stress in the surrounding rock is clearly transferred to the coal roadway. Figure 4(b) shows that the horizontal stress distribution in the roof and floor is asymmetrical after the excavation of the coal roadway and that the stress concentration area in the roof is shifted towards the coal roadway. From Figure 4(c), it can be concluded that the shear stress is asymmetrical and butterfly-shaped, and the stress concentration occurs at the corner of the tunnel. The influence of compressive shear stress on the roof upper corner and the floor lower corner of the floor of the drainage roadway is the "key part" of the roadway damage. Figure 4(d) shows that the plastic zone of the bottom gas extraction roadway remains basically unchanged. The radius of the plastic zone is approximately 1-2 m. The plastic zone extends 1 m into the upper rib, 1.5 m into the lower rib, and 2 m into the roof and floor. Therefore, the influence of coal roadway excavation on the plastic zone of the bottom gas extraction roadway is relatively small. Figures 4(e) and 4(f) show that the cumulative roof subsidence is 118.3 mm, the cumulative floor heave is 79.4 mm, and the cumulative approaches of the upper and lower ribs are 69 mm and 85.1 mm.

Figure 5 shows that the vertical stress distributions in the two ribs are basically the same and the upper rib stresses are slightly higher than the lower rib stresses. The peak stress in the upper rib is 26.5 MPa, which is 2.5 MPa less than that of the first disturbance, and this peak value occurs approximately 1.8 m into the surrounding rock of the roadway. The peak stress in the lower rib is 25.5 MPa, which is 3.5 MPa less than that of the first disturbance, and this peak value occurs 3.1 m into the surrounding rock of the roadway.

Figure 6 shows that the peak stress in the floor is higher than that in the roof. The peak value of the floor horizontal stress is 48 MPa, which is 6 MPa higher than the peak value

Table 1: Rock mechanics parameters.

Stratum	Thickness (m)	Compressive strength (MPa)	Elastic modulus (GPa)	Poisson ratio	Friction angle (°)	Density (kg·m^{-3})
Sandy mudstone	11	20	7.5	0.26	34	2500
Fine sandstone	8	45	15	0.22	38	2550
Sandy mudstone	3	20	7.5	0.26	34	2500
$Ji_{15\text{-}17}$ coal	4	8	1.4	0.32	26	1600
Sandy mudstone	5	20	7.5	0.26	34	2500
Limestone	19	56	15	0.19	40	2600
Mudstone	5	18.9	6.5	0.28	32	2300

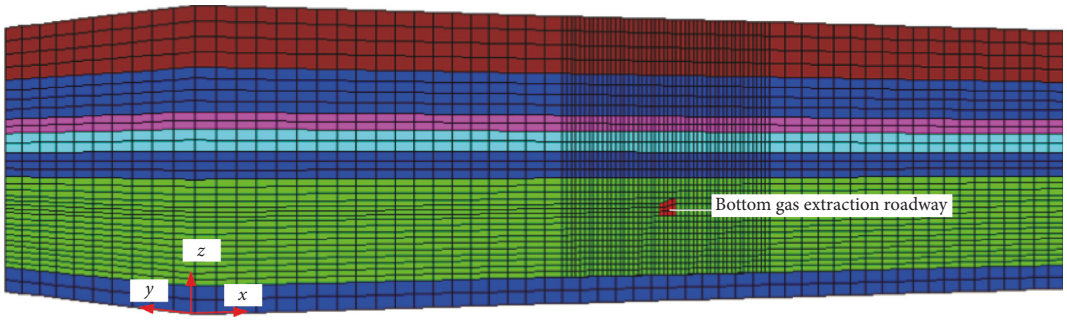

Figure 2: Numerical simulation model. Taking Pingbao Coal Mine as an example, the initial model of numerical simulation is established. The *X* direction is perpendicular to the medial axis of the bottom gas extraction roadway, and the *Y* direction is parallel to the medial axis of the bottom gas extraction roadway.

after the first disturbance, and the peak value occurs 3.65 m below the roadway floor. The peak value of the horizontal stress in the roof is 40.5 MPa, which is 1.5 MPa less than the peak value after the first disturbance. This peak value occurs 4.25 m into the surrounding rock of the roadway.

2.2.3. Stress and Deformation of the Surrounding Rock of a Bottom Gas Extraction Roadway after Mining Face Excavation. After mining of the coal face, another disturbance to the floor of the bottom gas extraction roadway will occur. The stress field, plastic zone extent, and displacement field in the surrounding rock in the floor of the bottom gas extraction roadway will be redistributed, as shown in Figure 7.

Figure 7(a) shows that a vertical stress redistribution occurs around the bottom gas extraction roadway after mining in the coal face. Under the influence of the lateral abutment pressure of the mining face, the stress to the lower rib of the roadway changes greatly, and the stress concentration is low, resulting in a state of pressure relief. Figure 7(b) shows that the horizontal stresses in the roof and floor are clearly asymmetrical and irregularly distributed. The roof is affected by the pressure relief of the mining face, and the stress concentration in the roof is low. Figure 7(c) shows that the shear stress has an asymmetrical butterfly-shaped distribution and that the stress concentration occurs at the corner of the roadway. The roof lower corner and the floor upper corner of the bottom gas extraction roadway are affected by the compressive shear stress, and the influence range is much larger than that of the area affected by the second disturbance. Figure 7(d) shows that the plastic zone around the bottom gas extraction roadway is clearly affected after mining because it is 0.5 m larger than that after the second disturbance. Figures 7(e) and 7(f) show the displacement of the roadway surface: the cumulative subsidence of the roof is 155 mm, the cumulative floor heave is 91.5 mm, and the cumulative extents of inward tilting of the upper and lower ribs are 83.6 mm and 104.2 mm.

Figure 8 shows that the vertical stresses in the two ribs of the surrounding rock of the bottom gas extraction roadway are quite different; the upper rib clearly has higher stresses than those in the lower rib. The peak stress to the upper rib of the bottom gas extraction roadway is 33.5 MPa, which is 7 MPa higher than that of the second disturbance, and the peak value occurs 2.45 m into the surrounding rock of the roadway. The peak stress to the lower rib of the bottom gas extraction roadway is 21.5 MPa, which is 4 MPa less than that of the second disturbance, and the peak value occurs 3.1 m into the surrounding rock of the roadway.

Figure 9 shows that the peak value of the horizontal stress in the floor is clearly higher than that in the roof after mining in the coal face. The peak horizontal stress in the floor of the bottom gas extraction roadway is 46 MPa, which is 2 MPa less than that after the second disturbance, and the peak value occurs 4 m below the floor of the roadway. The peak horizontal stress in the roof of the bottom gas extraction roadway is 33.5 MPa, which is 7 MPa less than that after the second disturbance. The peak value occurs approximately 4 m above the roof.

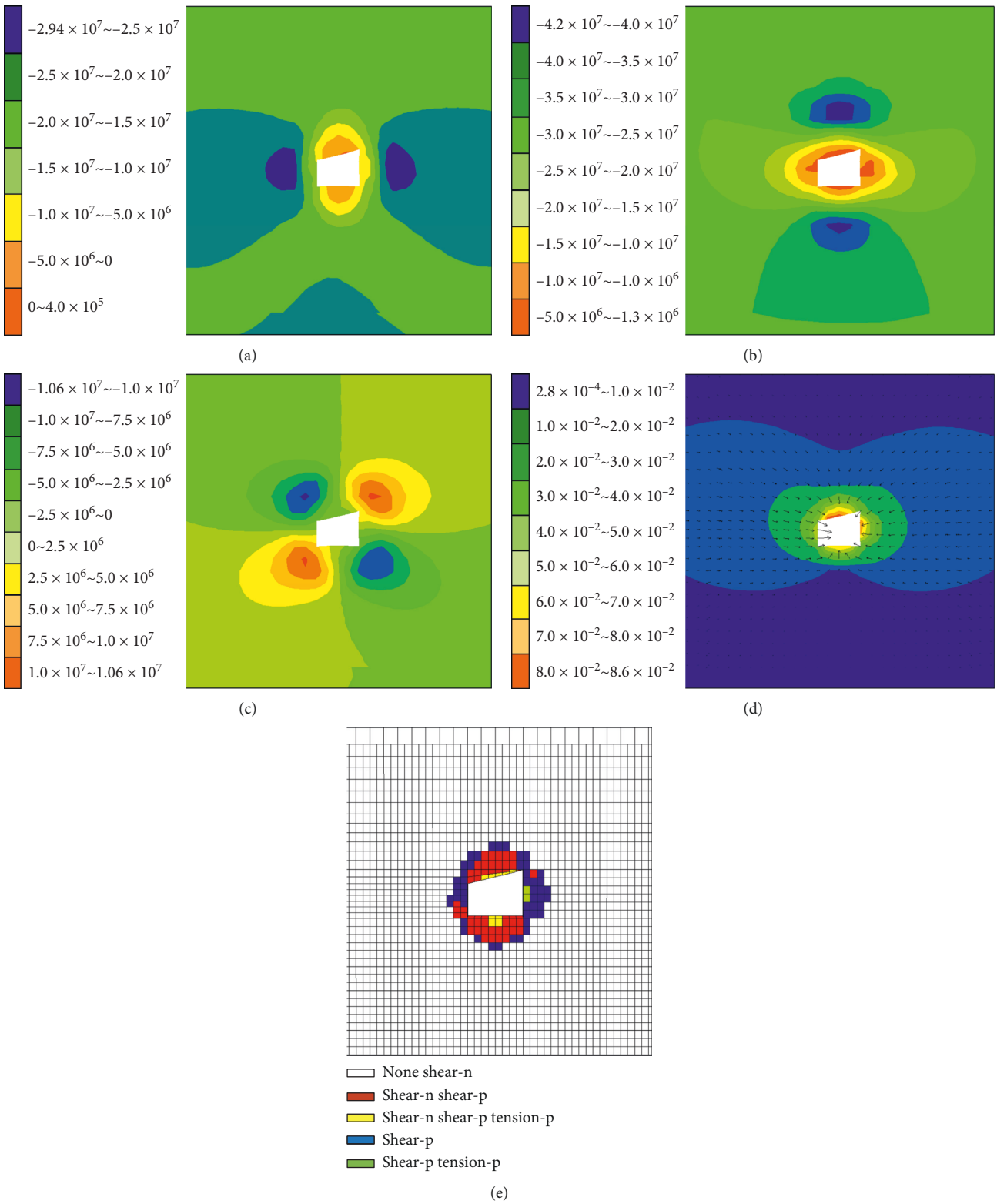

Figure 3: Stress field, displacement field, and plastic zone extent around a bottom gas extraction roadway after excavation. (a) Vertical stress distribution. (b) Horizontal stress distribution. (c) Shear stress distribution. (d) Distribution of displacement field. (e) Distribution of plastic zone.

The distribution of the stress and plastic zone in the roof and floor and two ribs of the bottom gas extraction roadway under three disturbances, namely, excavation of the bottom gas extraction roadway, excavation of the coal roadway, and mining of the coal face, are determined through simulation. Through a comparative analysis, the following conclusions

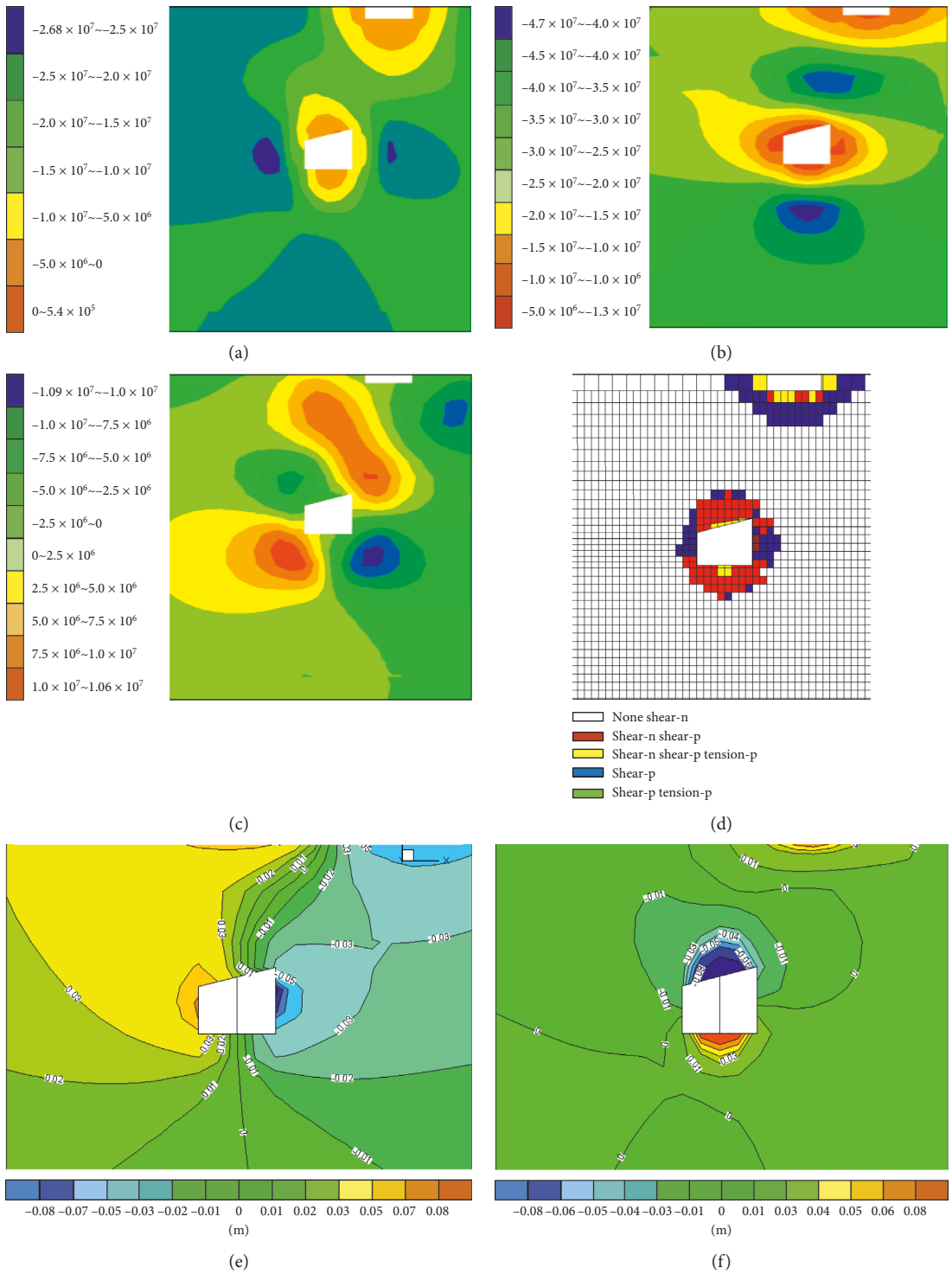

Figure 4: Stress field, displacement field, and plastic zone extent around the bottom gas extraction roadway after coal roadway excavation. (a) Vertical stress distribution. (b) Horizontal stress distribution. (c) Shear stress distribution. (d) Distribution of plastic zone. (e) Horizontal displacement distribution. (f) Vertical displacement distribution.

are drawn: (1) With the increase in the number of disturbances, the peak value of the vertical stress to the lower rib of the bottom gas extraction roadway gradually decreases, and the stress concentration gradually shifts deeper. The peak value of the vertical stress to the upper rib of the bottom gas extraction roadway first decreases and then increases, mainly due to the pressure relief of the floor after coal seam mining. (2) With continued mining, the peak horizontal stress of the floor of the bottom gas extraction roadway first increases and then decreases. After the roof coal seam is mined, the pressure relief is sufficient and the peak value of the horizonal stress to the roof of the bottom gas extraction roadway

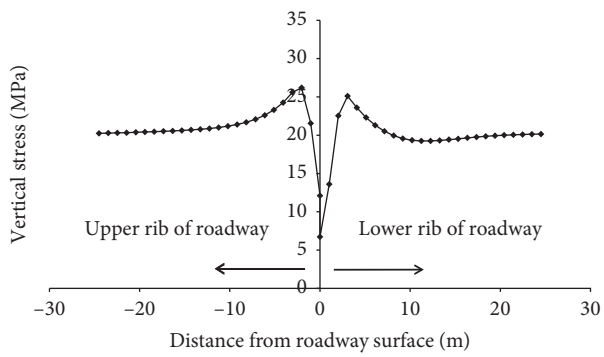

Figure 5: Vertical stress distribution on both ribs of bottom gas extraction roadway. The longitudinal axis represents the surface of upper (lower) rib of the bottom gas extraction roadway.

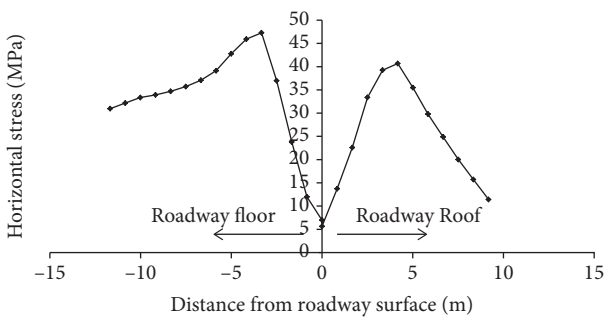

Figure 6: Horizontal stress distribution in the bottom gas extraction roadway roof and floor. The longitudinal axis represents the surface of roof (floor) of a bottom gas extraction roadway.

gradually decreases. (3) The four corners of the bottom gas extraction roadway concentrate shear stresses and are the key parts of the support. (4) With continued mining, the influence of the bottom gas extraction roadway excavation and coal roadway excavation on the plastic zone is small, and the average depth of the plastic zone is approximately 1.5 m. However, due to the disturbance of the mining face, the influence on the bottom gas extraction roadway is greater, and the average depth of the plastic zone is approximately 2 m. (5) With the increase in the number of disturbances, the surface displacement at the bottom gas extraction roadway increases and the deformation in the roof and lower rib of the bottom gas extraction roadway is larger than that in the bottom and upper ribs, respectively.

3. Analysis of Stress and Deformation Law of a Bottom Gas Extraction Roadway

According to the maximum horizontal stress theory [21, 22], the horizontal stress is usually greater than the vertical stress, and the stability of the roadway roof and floor is mainly affected by the horizontal stress. Therefore, after the excavation of the bottom gas extraction roadway, the vertical stress transfers to the ribs and the horizontal stress transfers to the roof and floor. With the disturbance of the overlying coal seam, the vertical and horizontal stresses around the bottom gas extraction roadway are redistributed and transferred to deeper depths. Vertical stress mainly affects the deformation of the ribs, while horizontal stress mainly affects the deformation of the roof and floor. The vertical distance between the bottom gas extraction roadway and overlying coal seam is 10 m, the horizontal distance between the bottom gas extraction roadway and coal roadway is 5 m, and outward staggered arranging is taken as the analysis object. According to the beam bending theory of material mechanics and the composite beam theory of bolt-mesh support design, the stress analysis of a bottom gas extraction roadway is carried out, as shown in Figure 10.

Assuming that the roof stratum of the bottom gas extraction roadway acts as a simply supported beam, the horizontal stress is F_s, the vertical stress is F_h, and the friction between roof strata is f, as shown in Figure 10. Then, the roof is simplified as a simply supported beam for force analysis, and the force situation is shown in Figure 11.

In Figure 11, it is assumed that q_1 is a simply supported beam (roof) subjected to a uniform load generated by rock dilatation deformation. The dead weight of the roof rock mass beam is G, and $F_A = F_s - 2f$ is the actual horizontal force of the simply supported beam. Assuming that the simply supported beam is not directly affected by the vertical stress (the vertical stress is transferred to the ribs of the roadway after excavation), the deflection calculation equation of any point of the beam can be obtained according to the superposition theory of bending deformation of material mechanics and the maximum deflection, i.e., the maximum subsidence of the roof can be obtained.

According to the superposition principle of bending deformation of beams, the deflection of beams under several loads is equal to the algebraic sum of deflection under each load alone [23]. Figure 11 shows that rock breaking force q_1, gravity G, and horizontal force F_A act on the roof of bottom gas extraction roadway. According to the superposition principle, the deflection of the roof is obtained as follows:

$$\omega_1 = \omega_{q_1} + \omega_G + \omega_{F_A}, \tag{1}$$

where ω_1 is the total displacement of the rock beam, ω_{q_1} is the displacement caused by the breaking-up force of the roof rock, ω_G is the displacement caused by the dead weight of the rock beam, and ω_{F_A} is the displacement caused by the actual horizontal force $(F_s - 2f)$.

The differential equation of the deflection curve of a beam is as follows [23]:

$$\frac{d^2\omega}{dx^2} = \frac{M}{EI}. \tag{2}$$

In equation (5), ω is the deflection, M is the bending moment, and I is the inertia moment.

Equations (3)–(5) are obtained by differential calculation of each load:

$$\omega_{q_1} = -\frac{q_1 x}{24EI_z}\left(l^3 - 2lx^2 + x^3\right), \tag{3}$$

$$\omega_G = -\frac{Gx}{48EI_z}\left(3l^2 - 4x^2\right), \tag{4}$$

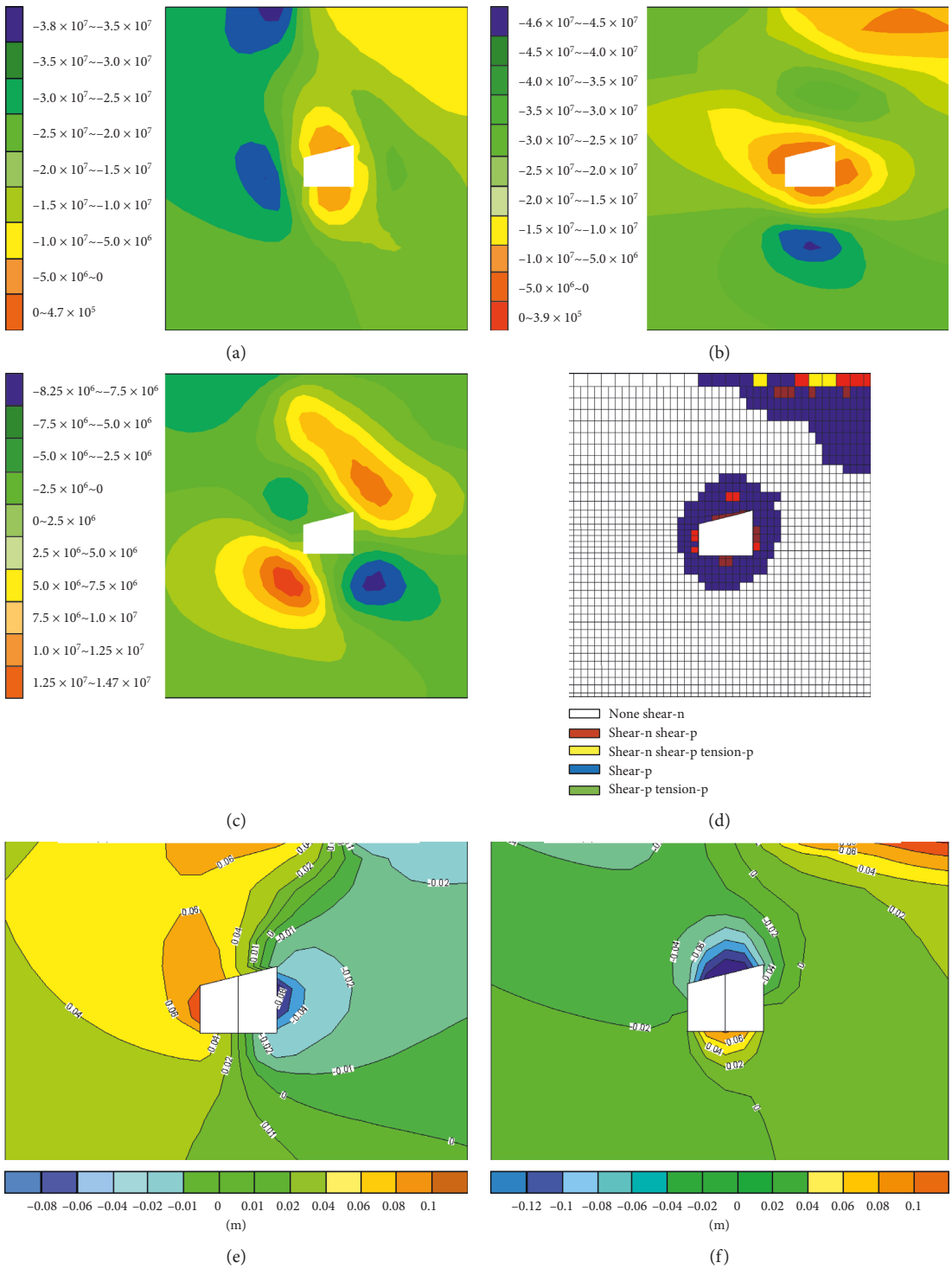

Figure 7: Stress field, displacement field, and plastic zone extent around the bottom gas extraction roadway after working face excavation. (a) Vertical stress distribution. (b) Horizontal stress distribution. (c) Shear stress distribution. (d) Distribution of plastic zone. (e) Horizontal displacement distribution. (f) Vertical displacement distribution.

$$\omega_{F_A} = -A \sin \frac{F_A}{EI_z} x + B \cos \frac{F_A}{EI_z} x. \tag{5}$$

The displacement at any point of the roof can be obtained by substituting equations (3)–(5) into (1). When $x = l/2$, the maximum deflection is reached, and equations (1)–(5) are used to determine the maximum roof subsidence:

$$\omega_{\max} = -\frac{5q_1 l^4}{384EI_z} - \frac{Gl^3}{48EI_z} - \frac{l}{2}\left(A \sin \frac{F_A}{EI_z} + B \cos \frac{F_A}{EI_z}\right), \tag{6}$$

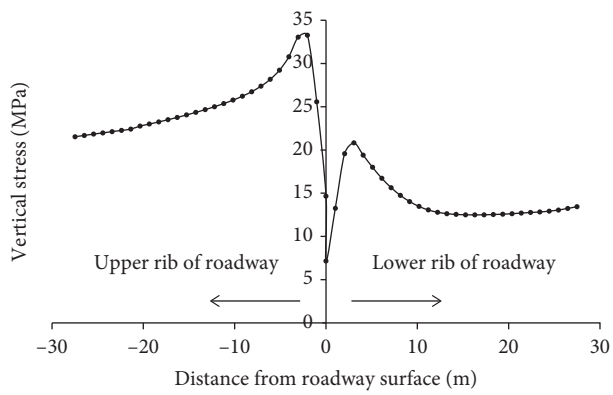

Figure 8: Vertical stress distribution on both ribs of bottom gas extraction roadway. The longitudinal axis represents the surface of upper (lower) rib of the bottom gas extraction roadway.

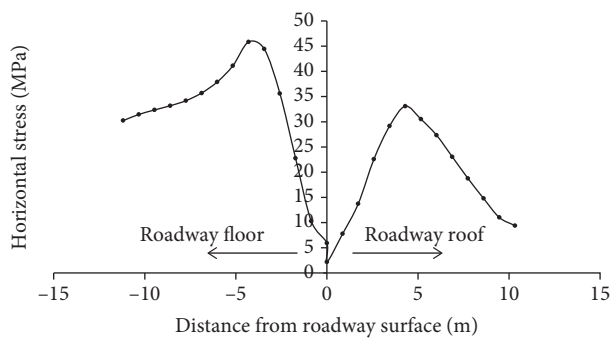

Figure 9: Horizontal stress distribution in the bottom gas extraction roadway roof and floor. The longitudinal axis represents the surface of roof (floor) of the bottom gas extraction roadway.

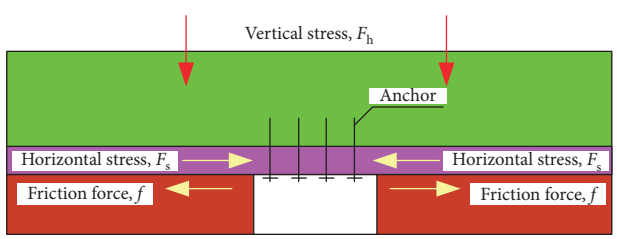

Figure 10: Simplified schematic diagram of a bottom gas extraction roadway. After the formation of bottom gas extraction roadway, it is mainly affected by vertical stress and horizontal stress.

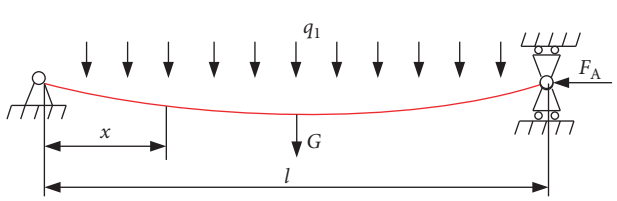

Figure 11: Simplified schematic diagram of a roof. Red curve represents roof of bottom gas extraction roadway. The roof of bottom gas extraction roadway is simplified as a simply supported beam.

where x is any point on a simply supported beam, E is the modulus of elasticity, and I_z is the moment of inertia of the simply supported beam, $I_z = bh^3/12$. According to the theory of a composite beam supported by bolts and mesh, h is the length of each bolt and b is the length of the row of bolts. The length of the beam, that is, the span of the bottom gas extraction roadway is l. A and B are integral constants.

Equation (6) shows that the factors affecting the displacement at any point in the beam with a bolt-mesh support form include the rock breaking force q_1, gravity G, and horizontal force F_A. When the roadway is disturbed by different sources, the influence of roof mining varies, so the value of q_1 also varies. With an increase in the disturbance frequency and intensity, the damage to the roof of the bottom gas extraction roadway increases, causing the roof subsidence to increase gradually. Thus, it is reasonable to explain that the roof subsidence of bottom gas extraction roadway under coal face mining disturbance is larger than that of bottom gas extraction roadway under coal roadway driving disturbance.

The effect of different disturbance forms on the floor is less than that on the roof, so the dilatancy deformation force q_2 of the floor is less than that of the roof. In addition, the gravity of the rock beam of the floor cannot be considered; therefore, under the same disturbance, the floor heave of the bottom gas extraction roadway is less than the roof subsidence.

After the roof is bent under force, the stress distribution in the roof will inevitably change. According to the distribution of the bending stress, in general, the maximum normal stress of the beam should occur on the section with the largest bending moment [23], that is, in the middle of the roof, and the maximum shear stress should occur at the end of the beam. The left half is taken as the research object, and the coordinate system is established with the fixed fulcrum on the left. The force is shown in Figure 12.

According to the stress analysis of Figure 11, the maximum bending moment of the beam occurs at $x = l/2$. The bending moment at the maximum deflection can be calculated from the force condition shown in Figure 12:

$$M_{\max} = F_A \omega_{\max} + \frac{Gl}{8} + \frac{q_1 l}{8}. \tag{7}$$

The maximum normal stress at the maximum bending moment is as follows:

$$\sigma_{\max} = \frac{M_{\max} y_{\max}}{I_z} = \frac{(F_A \omega_{\max} + (Gl/8) + (q_1 l/8)) y_{\max}}{I_z}, \tag{8}$$

where $y_{\max}$ is the farthest point between the simplified beam and the neutral plane.

The maximum shear stress is

$$\tau_{\max} = \frac{F_{\text{smax}} h^2}{8 I_z}, \tag{9}$$

where F_{smax} is the maximum shear force at the end of the beam.

Similarly, the deformation analysis of the rib of the roadway surrounding rock can also be based on the bending deformation theory of the beam mentioned above by simplifying the upper part as a fixed compression bar. In Figure 13, F_B is the pressure on both ends of the compression

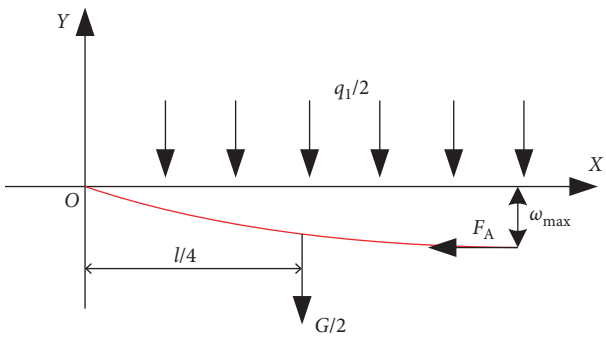

Figure 12: Simplified schematic diagram of the left half of the roof. Red curve represents the left half of the roof of the bottom gas extraction roadway.

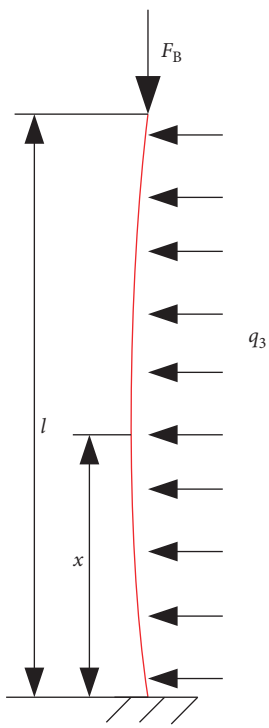

Figure 13: Simplified schematic diagram of the roadway ribs. Red curve represents the upper (lower) rib of the bottom gas extraction roadway. The rib of the bottom gas extraction roadway is simplified as a compression bar.

bar, $F_B = F_h + G$. After analysis, the deflection equation of any point on the rib is obtained (see equation (10), that is, the displacement equation).

Figure 13 shows that rock breaking force q_3 and vertical force F_B act on the rib of bottom gas extraction roadway. According to the superposition principle, the deflection of any point in the rib is obtained as follows:

$$\omega = -\left(A \sin \frac{F_B}{EI_z} x + B \cos \frac{F_B}{EI_z} x\right) - \frac{q_3 x}{24EI_z}\left(l^3 - 2lx^2 + x^3\right), \tag{10}$$

where x is any point on the compression bar, E is the modulus of elasticity, I_z is the moment of inertia, $I_z = bh^3/12$, l is the roadway height, and A and B are integral constants.

With the different disturbance forms, the lower rib is seriously disturbed by the coal seam and $q_4 < q_3$. Therefore, the lower rib approach is greater than the upper rib approach, and with more intense disturbance forms, the influence of mining on the bottom gas extraction roadway gradually increases, gradually increasing the displacement of the ribs.

Because the vertical stress F_h is less than the horizontal stress F_s, the deformation of the two ribs is less than the roof subsidence and floor heave. The stress magnitudes of the bending rib are consistent with the analysis method of the roof, which is not discussed here.

4. Control Measures of the Surrounding Rock of a Bottom Gas Extraction Roadway and Field Application

4.1. Supporting Technology. According to the deformation characteristics of the bottom gas extraction roadway and design calculations, it is proposed that the bottom gas extraction roadway should adopt anchor-net-cable and ladder beam support [24]. The roof bolts adopted are high-strength yielding bolts of 22 × 2400 mm, and the row spacing is 750 mm × 800 mm. A high-strength yielding bolt is adopted for the rib bolt, the type is 20 × 2400 mm, and the row spacing is 700 mm × 800 mm. The metal mesh is 6 mm steel mesh, with 80 × 80 mm, and the whole section of the mesh is connected. The type of anchor cable is 17.8 × 8300 mm, the size of a pallet is 300 mm × 300 mm × 16 mm, and the matching size is 120 mm × 120 mm × 10 mm. The spacing between rows is 1500 mm × 3200 mm. See Figure 14 for a sketch of the support. The bolts are matched with hemispherical washers, nylon or resin friction-reducing washers, and high-strength nuts.

4.2. Field Observation

4.2.1. Engineering Survey. The main coal seam in the Pingbao Coal Mine is the Ji15-17 coal seam, which is a thick coal seam. Its structure is simple and stable to relatively stable. The gas pressure of the coal seam is 1.38 MPa, which poses a risk of dangerous coal seam outburst. The direct floor of the Ji15-17 coal seam is mostly mudstone and sandy mudstone with an average thickness of 3.43 m. The 12030 coal face is 1621 m long in the strike direction and 140 m long along the inclination angle. The bottom gas extraction roadway is located 10 m under the floor of the coal seam but not directly below the coal roadway. The horizontal offset is 5 m, as shown in Figure 15.

4.2.2. Field Observation and Analysis. The above numerical simulation and theoretical analysis are used to study the deformation characteristics of bottom gas extraction roadways subjected to multiple disturbances. To further verify the deformation law and support effect, field observations are carried out on the influence of three stages, namely, the bottom gas extraction roadway excavation, coal roadway excavation, and working face mining, on the bottom gas extraction roadway in the 12030 coal mining face of the Pingbao Coal Mine. The layout chart of displacement observation point is shown in Figure 16.

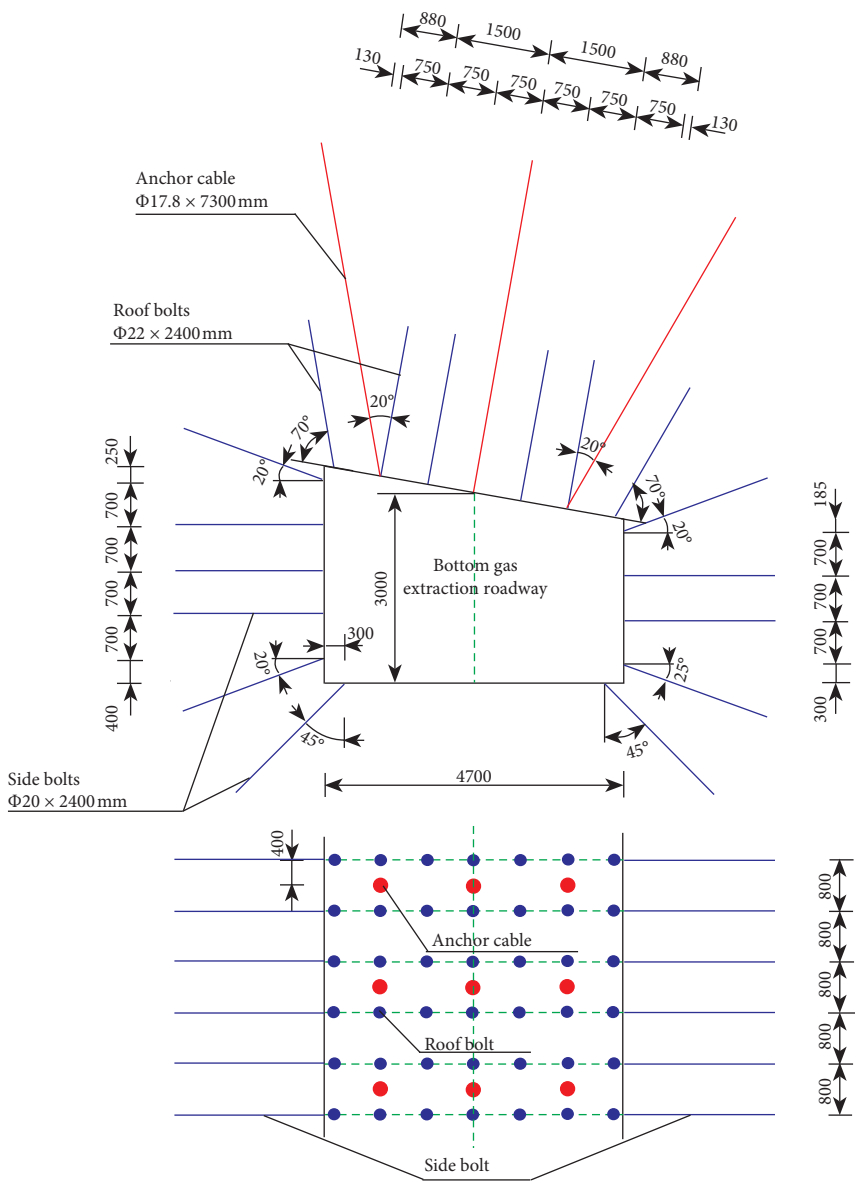

Figure 14: Bottom gas extraction roadway support diagram. The upper and lower parts are the cutaway view and the top view of the bottom gas extraction roadway, respectively.

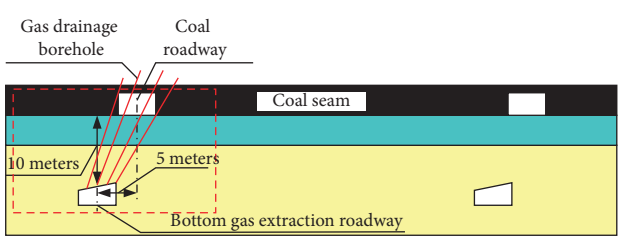

Figure 15: Schematic diagram of bottom gas extraction roadway layout. The bottom gas extraction roadway is located 10 m under the floor of the coal seam but not directly below the coal roadway. The horizontal offset is 5 m.

(1) Surface Displacement Observation of Bottom Gas Extraction Roadway. After the excavation of the bottom gas extraction roadway, the displacement observation of the roadway is carried out until the deformation of the roadway is basically stable. The cumulative approaches of the upper and lower ribs are 41 mm and 43 mm, respectively. The cumulative displacements of the roof and floor are 62 mm and 92 mm, respectively.

During the driving of coal roadway, the displacement observation point is arranged 40 m ahead of the coal roadway in the bottom gas extraction roadway, and the observation is stopped only after the surface displacement of the bottom gas extraction roadway is basically unchanged. The cumulative displacements of the upper and lower ribs of the bottom gas extraction roadway are 56 mm and 65 mm, respectively, and the cumulative displacements of the roof and floor are 133 mm and 124 mm, respectively.

During the coal face mining period, the original measuring points are used. After the surface displacement of the bottom gas extraction roadway basically remains unchanged, the observation is stopped. When disturbed by the

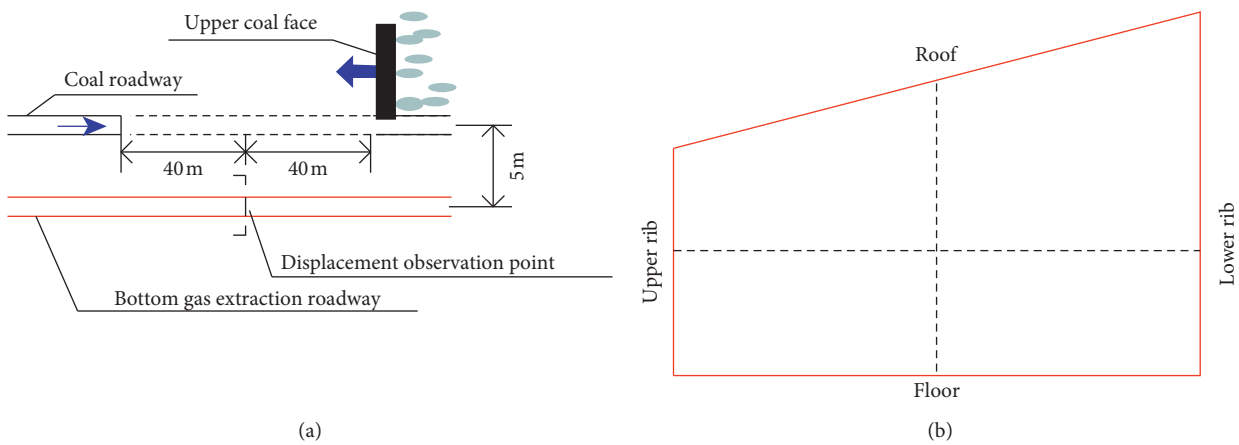

Figure 16: Layout chart of displacement observation point. (a) The position relation between observation points and coal roadway and mining face. (b) Crossing method for observing surface displacement of bottom gas extraction roadway.

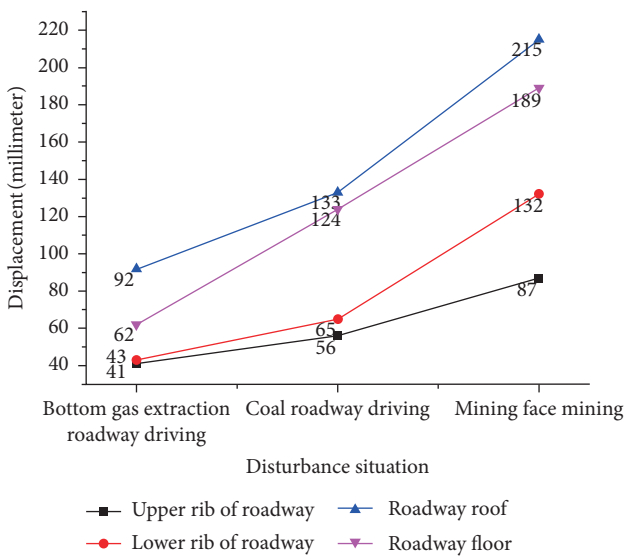

Figure 17: Surface displacement of the bottom gas extraction roadway in different disturbance periods. The transverse axis represents the order of disturbance, and the longitudinal axis represents the displacement of the observation points on the surface of the bottom gas extraction roadway.

Table 2: Borehole images.

Surrounding rock image	Hole depth (m)	Surrounding rock zone
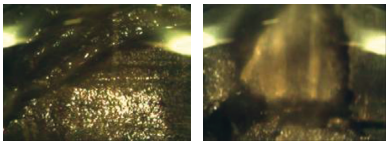	0~0.6	Crushing zone
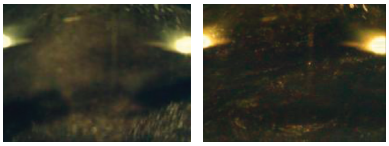	0.6~2	Fracture zone
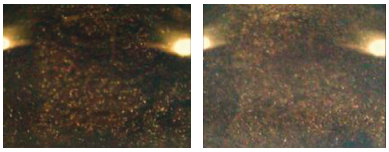	2~3	Stability zone

coal face, the cumulative displacements of the upper and lower ribs of the bottom gas extraction roadway are 87 mm and 132 mm, respectively, and the cumulative displacements of the roof and floor are 215 mm and 189 mm, respectively.

The field observation shows that the roof subsidence is greater than the floor heave and that the lower rib displacement is larger than the upper rib displacement after mining disturbance of overlying coal seam. This result is basically consistent with the conclusion of the numerical simulation and theoretical analysis, and the roadway deformation is within the allowable range. The observation results are shown in Figure 17.

(2) Observation of Surrounding Rock Fragmentation. After mining in the coal face, a 3 m deep hole is drilled directly above the observation point, and pictures are taken in different areas by using video recordings (Table 2). When it is located at 2 m depth, the surrounding rock is basically free of fragmentation and cracks, which is consistent with the results of the numerical simulation, proving that the support method can effectively control the stability of the surrounding rock of the bottom gas extraction roadway.

5. Conclusion

Based on the research background of a bottom gas extraction roadway in the Pingbao Coal Mine, the deformation characteristics of a bottom gas extraction roadway disturbed by bottom gas extraction roadway excavation, coal roadway

excavation, and working face mining are analysed by numerical simulation, and the stress variation around the bottom gas extraction roadway is analysed. The following conclusions are drawn:

(1) With the increase in the number of disturbances, the stress concentration in the lower rib and roof of the bottom gas extraction roadway gradually decreases and transfers to deeper rock. The stress in the floor first increases and then decreases, while the upper rib is opposite. The influence of bottom gas extraction roadway excavation and coal roadway excavation has little effect on the plastic zone of bottom drainage roadway, and the average depth of plastic zone is approximately 1.5 m. With the influence of coal face mining, the average depth of the plastic zone reaches approximately 2 m. The surface displacement of the bottom gas extraction roadway increases with the number of disturbances, and the deformation of the roof and lower rib of the bottom gas extraction roadway is larger than that of the floor and upper rib, respectively.

(2) By analysing the stress condition around the bottom gas extraction roadway, the deformation characteristics of the bottom gas extraction roadway under multiple disturbances are reasonably explained, and the methods for calculating the maximum displacement, the maximum normal stress, and the maximum shear stress on the surface of the bottom gas extraction roadway are obtained.

(3) The supporting technology of using anchor-net-cable and ladder beam support is put forward and applied to the bottom gas extraction roadway of a 12030 mining face in the Pingbao Coal Mine; this technology effectively controls the surface displacement of the bottom gas extraction roadway and the surrounding rock breakage.

Data Availability

The rock mechanics parameters used to support the findings of this study are included within the article. The numerical simulation analysis data and field observation data used to support the findings of this study are available from the corresponding author upon request.

Conflicts of Interest

The authors declare that there are no conflicts of interest regarding the publication of this paper.

Acknowledgments

This work was carried out with funding from the National Natural Science Foundation of China (grant nos. 51674103, 51304070, and U1361205). The authors wish to thank the organization for the support provided.

References

[1] Y. P. Cheng and Q. X. Yu, "Development of regional gas control technology for Chinese coal mines," *Journal of Mining and Safety Engineering*, vol. 24, no. 4, pp. 363–390, 2007.

[2] I.-L. Cioca and R. I. Moraru, "Explosion and/or fire risk assessment methodology: a common approach, structured for underground coalmine environments/metoda szacowania ryzyka wybuchu i pożarów: podejście ogólne, dostosowane do środowiska kopalni podziemnej," *Archives of Mining Sciences*, vol. 57, no. 1, pp. 53–60, 2012.

[3] H. X. Zhou, H. Dai, and C. G. Ge, "Quality and quantity of pre-drainage methane and responding strategies in Chinese outburst coal mines," *Arabian Journal of Geosciences*, vol. 9, no. 6, 2016.

[4] H. F. Wang, Y. P. Chen, and L. Wang, "Regional gas drainage techniques in Chinese coal mines," *International Journal of Mining Science and Technology*, vol. 22, no. 6, pp. 873–878, 2012.

[5] Q. L. Yao, X. H. Li, F. Pan, T. Wang, and G. Wang, "Deformation and failure mechanism of roadway sensitive to stress disturbance and its zonal support technology," *Shock and Vibration*, vol. 2016, no. 1155, Article ID 1812768, 14 pages, 2016.

[6] S. Y. Zhu, Z. Q. Jiang, P. Yao, and W.-G. Xiao, "Application of analytic method in calculating floor stress of a working face," *Journal of Mining and Safety Engineering*, vol. 24, no. 2, pp. 192–195, 2007.

[7] F. C. Santos and Z. T. Bieniawski, "Floor design in underground mines," *Rock Mechanics and Rock Engineering*, vol. 22, no. 4, pp. 226–249, 1989.

[8] A. Afrouz, F. P. Hassani, and M. J. Scoble, "Geotechnical assessment of the bearing capacity of coal mine floors," *International Journal of Mining and Geological Engineering*, vol. 6, no. 4, pp. 297–312, 1988.

[9] P. L. Gong, Y. Q. Hu, Y. S. Zhao et al., "Three-dimensional simulation study on law of deformation and breakage of coal floor on mining above aquifer," *Chinese Journal of Rock Mechanics and Engineering*, vol. 24, no. 23, pp. 4396–4402, 2005.

[10] Y. B. Guan, H. M. Li, and J. C. Lu, "Research of no. 9 coal seam floor's fracture regularity in Xiandewang coal mine," *Journal of China Coal Society*, vol. 28, no. 2, pp. 121–125, 2003.

[11] W. B. Xie, Z. F. Shi, X. X. Chen, and S.-L. Lu, "Stability analyses of roadway surrounding rock induced by overhead mining," *Journal of China University of Mining and Technology*, vol. 33, no. 1, pp. 82–85, 2002.

[12] S. L. Lu, "Selection of horizontal distance x between roadway and the edge of its upper pillar," *Journal of China University of Mining and Technology*, vol. 22, no. 1, pp. 1–7, 1993.

[13] J. C. Zhang, Y. Z. Zhang, and T. Q. Liu, *Rock Mass Permeability and Coal Mine Water Inrush*, Geological Publishing House, Beijing, China, 1997, in Chinese.

[14] J. Sun, "Failure characteristics of floor "three-zone" along the inclined direction of coal seam," *Journal of Mining and Safety Engineering*, vol. 31, no. 1, pp. 115–121, 2014.

[15] W. Zhou, P. Zhang, R. Wu, and X. Hu, "Dynamic monitoring the deformation and failure of extra-thick coal seam floor in deep mining," *Journal of Applied Geophysics*, vol. 163, pp. 132–138, 2019.

[16] H. Zhang, L. Wang, F. Gao, and H. Yang, "Numerical simulation study on the influence of the ground stress field on the

stability of roadways," *Mining Science and Technology (China)*, vol. 20, no. 5, pp. 707–711, 2010.

[17] B. S. Zhang, S. S. Yang, L. X. Kang, and Y. D. Zhai, "Discussion on method for determining reasonable position of roadway for ultra-close multi-seam," *Chinese Journal of Rock Mechanics and Engineering*, vol. 27, no. 1, pp. 97–101, 2008.

[18] H. Zhang, J. Cao, and M. Tu, "Floor stress evolution laws and its effect on stability of floor roadway," *International Journal of Mining Science and Technology*, vol. 23, no. 5, pp. 631–636, 2013.

[19] X. J. Yang, C. W. Hu, M. C. He et al., "Study on presplitting blasting the roof strata of adjacent roadway to control roadway deformation," *Shock and Vibration*, vol. 2019, no. 1155, Article ID 3174898, 16 pages, 2019.

[20] R. Gu and U. Ozbay, "Numerical investigation of unstable rock failure in underground mining condition," *Computers and Geotechnics*, vol. 63, pp. 171–182, 2015.

[21] Z. Liang, B. Gong, and W. Li, "Instability analysis of a deep tunnel under triaxial loads using a three-dimensional numerical method with strength reduction method," *Tunnelling and Underground Space Technology*, vol. 86, pp. 51–62, 2019.

[22] Z. Mu, G. Liu, J. Yang et al., "Theoretical and numerical investigations of floor dynamic rupture: a case study in Zhaolou Coal Mine, China," *Safety Science*, vol. 114, pp. 1–11, 2019.

[23] R. C. Hibbeler, *Mechanics of Materials*, Publishing House of Electronics Industry, Beijing, China, 2006, in Chinese.

[24] C. Q. Ma, P. Wang, L. S. Jiang, and C. S. Wang, "Deformation and control countermeasure of surrounding rocks for water-dripping roadway below a contiguous seam goaf," *Processes*, vol. 6, no. 7, p. 77, 2018.